Diamond & Related Materials 92 (2019) 86–91

Contents lists available at ScienceDirect

Diamond & Related Materials

journal homepage: www.elsevier.com/locate/diamond

Linear magneto-electron-light interaction in ultranarrow armchair graphene and boronitrene nanoribbons

Nguyen D. Hien[a,b], Kavoos Mirabbaszadeh[c,*], Mohsen Yarmohammadi[c,*], Bui D. Hoi[d,*]

[a] Laboratory of Magnetism and Magnetic Materials, Advanced Institute of Materials Science,Ton Duc Thang University, Ho Chi Minh City, Viet Nam
[b] Faculty of Applied Sciences, Ton Duc Thang University, Ho Chi Minh City, Viet Nam
[c] Department of Energy Engineering and Physics, Amirkabir University of Technology, Tehran, Iran
[d] Center for Theoretical and Computational Physics and Department of Physics, University of Education, Hue University, Hue City, Viet Nam

A B S T R A C T

Using the synergy between the tight-binding model and the Green's function approach, this paper deals with the linear magneto-electron-light interaction in ultranarrow armchair graphene and boronitrene nanoribbons theoretically. In particular, we study the effect of ribbon width and the magnetic field on the refractive index, the absorption coefficient, and the extinction coefficient of abovementioned structures. Here, we reveal that there exists an increasing behavior for *static* refractive index of both structures when the ribbon width and the magnetic field are increased, whereas the *dynamical* refractive index increases (oscillates) in average with the ribbon width (magnetic field) at different light frequencies. We further show that the effect of ribbon width (magnetic field) on the absorption coefficient is generally increasing (oscillating) when the photon energy is altered. No refraction and absorption is reported at high enough photon frequencies independent of the ribbon width and the magnetic field strength. In addition, we find that the scattering process in the presence of the magnetic field manifests itself in the extinction coefficient. This information provides insights into the engineers in determining which ribbon width and magnetic field strength to use in the solar cell designs.

1. Introduction

Appealing counterparts of graphene have recently triggered numerous theoretical and experimental studies due to their valuable physical properties in future real applications in the optoelectronic industry [1-12]. Graphene nanoribbons (GNRs) as one-dimensional (1D) counterparts of graphene exhibit a practical utilization in nano-optoelectronic devices [13-15] depending on the edge shape and size [16-26], resulting in formation of different standing electronic waves of Dirac fermions. However, not only the ribbon width and the shape of edges provide successful uses of GNRs, but also the effect of external perturbations may have crucial roles in the information obtained [27-29]. In order to achieve a better efficiency, i.e. a higher photocurrent in optoelectronic devices as well as spintronic devices, GNRs are proper candidates, as proven in Refs. [2,3,30,31].

Similar to graphene, other hexagonal nanomaterials such as MoS_2 [32], SiC [33], BN [34] have been widely fabricated and synthesized by different methods. The hexagonal BN, so-called boronitrene is an insulator, providing different properties both qualitatively and quantitatively than graphene due to the quantum confinement effects. Thus, boronitrene nanoribbons (BNNRs) by cutting the BN sheet should also exhibit different features than GNRs. However, due to the wide band gap of boronitrene, the range of logic applications based on boronitrene is widen [35-37]. To have exotic optical properties of devices based on low-dimensional nanomaterials, it has been shown that host electron-light interaction can be influenced under external *electronic* perturbations, see Refs. [27,38-53].

While there are numerous works on 1D systems in the presence of electronic perturbations, to the best of our knowledge, a few studies have been focused on the *magnetic* effects on the electron-light interaction in 1D materials, see Refs. [54-58]. In the optical response, the magnetic field leads to fascinating features [27,28,59]. Here, we take into account the magnetic field effect on both intraband and interband parts of the optical responses such as refractive index, the absorption coefficient, and the extinction coefficient at finite temperature and fixed wave vector transfer of incident light. We use the linear response theory to find that optical properties are highly more sensitive to the magnetic perturbations in the intraband regime of the response function than the interband ones. The Green's function approach is applied to describe the quantum correlation functions through charge density-charge density interactions. Calculations are carried out in the tight-binding model. In addition to the magnetic field, the ribbon width is varied to predict a response for more realistic systems. It is obvious that the competition between π-electrons in GNRs and BNNRs and the

* Corresponding authors.
E-mail addresses: nguyendinhhien@tdtu.edu.vn (N.D. Hien), mirabbas@aut.ac.ir (K. Mirabbaszadeh), my69@aut.ac.ir (M. Yarmohammadi), buidinhhoi@hueuni.edu.vn (B.D. Hoi).

https://doi.org/10.1016/j.diamond.2018.12.010
Received 14 November 2018; Received in revised form 8 December 2018; Accepted 12 December 2018
Available online 23 December 2018

external magnetic field provided by the Peierls phase factor yields nice information about the *linear* optical properties of 1D nanoribbons. We have calculated both real and imaginary parts of the dielectric function and then optical quantities.

The paper is organized as follows: Section 2 outlines briefly the semi-empirical tight-binding Hamiltonian model as well as the coupling between the magnetic field and the host electrons subjected to a photon beam ($\hbar\omega$, $\vec{q}$) using the Green's function technique. In Section 3, we use the Green's functions obtained to the investigation of the dielectric response function. In Section 4, we present and discuss our findings. Finally, in Section 5, conclusions are summarized besides the discussion for future applications.

2. Semi-empirical tight-binding model and Green's function theory

In this section, we intend to set up the theory required in the present work in order to express the dynamics of Dirac fermions based on the tight-binding Hamiltonian model. We are interested in armchair GNRs (aGNRs) much more than the zigzag ones because the electronic phase in aGNRs can be tuned much more than zigzag ones. In general, aGNRs can be divided into two families: {$n = 3p$ and $n = 3p + 1$} and $n = 3p + 2$ (n being the ribbon width) corresponding to the semiconductor and metallic phases, respectively, while all aBNNRs are insulator/semiconductor [7,27]. Herein, we focus only on the first family and we postpone the latter to our future researches. However, the details of transport in metallic aGNRs can be found in numerous works such as Ref. [60]. The empirical model consists of the nearest-neighbor hopping terms and the perpendicular magnetic field term $\vec{B} = \mathcal{B}\hat{e}_z$ applied to the quasi-1D armchair nanoribbons (a-NRs). In our formulation, we apply the periodic conditions (transnational symmetry) along the y (x) direction (see Fig. 1) Thus, the total Hamiltonian is described by

$$\hat{\mathcal{H}} = \sum_{i,\sigma} [\varepsilon_0^{\mathrm{A}} \hat{a}_{i,\sigma}^{\dagger}\hat{a}_{i,\sigma} + \varepsilon_0^{\mathrm{B}} \hat{b}_{i,\sigma}^{\dagger}\hat{b}_{i,\sigma}] - t_{p_z} \sum_{\langle i,j\rangle,\sigma} \hat{a}_{i,\sigma}^{\dagger}\hat{b}_{j,\sigma} - g\mu_{\mathrm{B}}\mathcal{B}/2 \sum_{i} [\hat{a}_{i,\uparrow}^{\dagger}\hat{a}_{i,\downarrow} + \hat{b}_{i,\uparrow}^{\dagger}\hat{b}_{i,\downarrow}] + \mathrm{H.c.}, \quad (1)$$

where $\hat{a}_{i,\sigma}/\hat{b}_{i,\sigma}$ ($\hat{a}_{i,\sigma}^{\dagger}/\hat{b}_{i,\sigma}^{\dagger}$) stands for the annihilation (creation) operator for the Dirac fermion at i-th site of the lattice with spin σ. The coefficient t_{p_z} of about 3.03 eV and 1.95 eV in the second term is the hopping integral energy between nearest-neighbor atoms with on-site energy

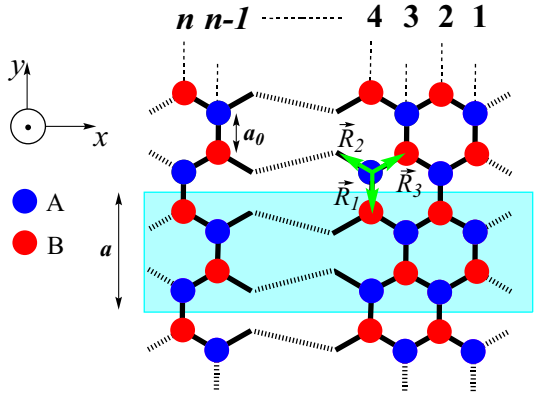

Fig. 1.) Sketch of top view of n-aNRs. Different colors of atoms imply to A (blue) and B (red) sublattices. The bond length between A and B atoms is denoted by a_0. The unit cell is shown with the shadowed box and $a = 3a_0$ is the unit cell width. Vectors $\vec{R}_{\{1,2,3\}}$ and the symbol ⊙ stand for the nearest-neighbors and the applied Zeeman magnetic field direction, i.e. the z direction, respectively. (For interpretation of the references to color in this figure legend, the reader is referred to the web version of this article.)

$\varepsilon_0^{\mathrm{A(B)}} = 0(0)$ eV and $\varepsilon_0^{\mathrm{A(B)}} = 0(-4.57)$ eV for GNRs and BNNRs, respectively [61,62]. In the third term, the magnetic field is introduced by the parameters g, μ_{B}, and $\mathcal{B}$ as the Lande g-factor, the Bohr magneton, and the magnetic field strength, respectively.

The effect of magnetic field on the orbital states of valence band maximum (VBM) and the conduction band minimum (CBM) is given by the Peierls phase factor $\Delta\Phi_{u,m}$ as $t_{p_z}^{u,m} = t_{p_z} e^{2\pi \mathrm{i}\Delta\Phi_{u,m}}$. The phase factor appearing in $t_{p_z}^{u,m}$ is calculated by a line integral of the vector potential $\vec{A} = (0, \mathcal{B}_z x)$ (Landau gauge) via [28,62,63]

$$\Delta\Phi_{u,m} = \frac{e}{h} \int_{\vec{R}_u}^{\vec{R}_m} d\vec{l}\cdot\vec{A}. \quad (2)$$

where e, h, $\vec{R}_1 = (0, -1)a_0$, $\vec{R}_2 = (-1, \sqrt{3})a_0/2$, and $\vec{R}_3 = (1, \sqrt{3})a_0/2$ with $a_0 = |\vec{R}_{u,m}|$ are the electron charge, the Planck constant, and vectors corresponding to the nearest-neighbors atoms, respectively (see Fig. 1).

To formulate the tight-binding model in the reciprocal space, we transform the annihilation and creation operators in Eq. (1) to the reciprocal space using the Fourier transformation. To this end, we use the basis sets $\psi_A(k_x,k_y)$ and $\psi_B(k_x,k_y)$ for sublattice A and B, respectively. Each index site i in Fig. 1 can be labelled with two other indices m and sublattices A_l and B_l for $l \in [1,n]$. Thus, we use

$$\hat{c}_{k_x,k_y}^{\dagger} = \frac{1}{\sqrt{N_c}} \sum_{m=1}^{N_c} \sum_{l=1}^{n} e^{\mathrm{i}k_x x_m} \psi_{\mathrm{c}}(l, k_y)\hat{c}_{l,m}^{\dagger}, \quad (3)$$

where c =A/B, N_c is the number of unit cells, and x_m uses for the position of m-th unit cell containing $2n$ atoms along the x axis. The wave functions for the y direction can be calculated utilizing the hard-wall boundary conditions [64],

$$\psi_{\mathrm{c}}(l, k_y) = \sin(\sqrt{3}a_0 k_y l/2), \quad (4)$$

with the discretized vertical wave vector $k_y = 2z\pi/(\sqrt{3}a_0[n + 1])$, where $z = \{1,2,3,\ldots n\}$. By diagonalizing the Hamiltonian in the reciprocal space, the electronic band structure can be calculated as

$$\mathcal{E}_{\nu}^{\sigma}(k_x, z) = \frac{\varepsilon_0^{\mathrm{A}} + \varepsilon_0^{\mathrm{B}}}{2} + \nu\sqrt{|\phi(k_x, z)|^2 + \left(\frac{\varepsilon_0^{\mathrm{A}} - \varepsilon_0^{\mathrm{B}}}{2}\right)^2} - \sigma g\mu_{\mathrm{B}}\mathcal{B}, \quad (5)$$

where the structure factor $\phi(k_x,z)$ is defined by

$$\phi(k_x, z) := -\sum_{u,m} \sum_{\vec{k}\in \mathrm{FBZ}} t_{p_z}^{u,m} e^{-\mathrm{i}\vec{k}\cdot\vec{R}_{u,m}}, \quad (6)$$

for the momenta $\vec{k} = (k_x, k_y)$ belonging to the first Brillouin zone (FBZ) of aNRs. The electronic band structure of 7-aNRs in the *absence* of the magnetic field are presented in the left panel of Fig. 2, showing an electron-hole symmetry in the VBM and CBM of the 14-band structures. 7-aGNR (7-aBNNR) is a semiconductor (insulator) with the band gap of about 1.5 (4.5) eV in good agreement with Refs. [61,62,65]. Another electronic property is the electronic density of states (DOS), which connects to the auto-correlation function between carriers in different and the same sublattices.

To this end, we calculate the *Green's function* elements within the Matsubara formalism [66] for $\{\alpha,\beta\}\in\{A,B\}$,

$$G_{\alpha\beta}^{\sigma}(t', k_x) = -\langle \mathcal{T}_{t'}[\hat{c}_{k_x,\alpha}^{\sigma}(t')\hat{c}_{k_x,\beta}^{\dagger,\sigma}(0)]\rangle,$$
$$G_{\alpha\beta}^{\sigma}(\mathrm{i}\omega_{\mathcal{F}}, k_x) = \int_0^{1/k_{\mathrm{B}}T} e^{\mathrm{i}\omega_{\mathcal{F}}t'} G_{\alpha\beta}^{\sigma}(t', k_x)dt'. \quad (7)$$

where t' is the imaginary time, the symbol $\mathcal{T}$ stands for the time-ordering operator, and $\omega_{\mathcal{F}} = (2\mathcal{F} + 1)\pi k_{\mathrm{B}}T$ is the fermionic Matsubara frequency (k_{B} being the Boltzmann constant and T is the absolute temperature). Finally, by means of tracing over the imaginary part of Green's function, DOS for $\mathrm{i}\omega_{\mathcal{F}} \to \mathcal{E} + i\eta$ is calculated by

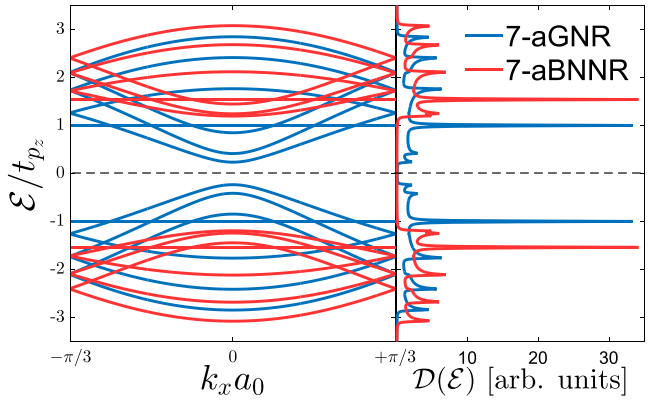

Fig. 2. The electronic band structure (left panel) and density of states (right panel) of 7-aNRs. The band gap is of about 1.5 eV and 4.5 eV for 7-aGNR and 7-aBNNR, respectively. The dashed horizontal line is the Fermi level.

$$\mathcal{D}(\mathcal{E}) = -\frac{1}{\pi N_c}\sum_{\sigma,\alpha,k_x}\mathrm{Im}[G^{\sigma}_{\alpha\alpha}(\mathcal{E}+\mathrm{i}\eta, k_x)]. \tag{8}$$

where $\eta = 30\,\mathrm{meV}$ is the broadening factor. The electronic DOS is shown in the right panel of Fig. 2 for both 7-aGNR and 7-aBNNR. The macroscopically degenerate states in the valance and conduction bands refer to the van Hove singularities in the electronic DOS. In the next section, we will focus on the dynamical response function of the systems using the Green's functions derived in Eq. (7) in order to describe the optical properties of the systems subjected to a photon beam and the magnetic field.

3. Dielectric response function

The main features of our study are given by the dielectric response function of the system subjected to an applied photon beam and magnetic field at a constant temperature. Let us first calculate the density-density response function within the linear response theory [66],

$$\epsilon(\mathrm{i}\omega_p, q_x) = -\int_0^{1/k_BT} dt' e^{\mathrm{i}\omega_p t'}\sum_{\sigma}\langle \mathcal{T}_{t'}[\hat{\rho}^{\sigma}(q_x, t') \times \hat{\rho}^{\sigma}(-q_x, 0)]\rangle, \tag{9}$$

where $\omega_p = 2p\pi k_B T$ is the bosonic Matsubara frequency and $\hat{\rho}^{\sigma}(q_x)$ refers to the charge density operator, defined by

$$\hat{\rho}^{\sigma}(q_x) = \frac{1}{N_c}\sum_{k_x,l}[\hat{c}^{\dagger,\sigma}_{Al,k_x+q_x}\hat{c}^{\sigma}_{Al,k_x} + \hat{c}^{\dagger,\sigma}_{Bl,k_x+q_x}\hat{c}^{\sigma}_{Bl,k_x}], \tag{10}$$

Thus using the Wick's theorem [66], each element of $\epsilon(\mathrm{i}\omega_p,q_x)$ is obtained via

$$\epsilon_{\alpha\beta}(\mathrm{i}\omega_p, q_x) = \frac{k_BT}{N_c}\sum_{k_x,\sigma,\mathcal{F}} G^{\sigma}_{\alpha\beta}(\mathrm{i}\omega_p + \mathrm{i}\omega_{\mathcal{F}}, k_x + q_x) \times G^{\sigma}_{\beta\alpha}(\mathrm{i}\omega_{\mathcal{F}}, k_x), \tag{11}$$

in which we deal with the Green's functions derived in Eq. (7). From Eq. (11), one figures out that the response function $\epsilon(\omega,q_x)$ has two real and imaginary parts, let's call them $\epsilon_1(\omega,q_x)$ and $\epsilon_2(\omega,q_x)$, respectively, i.e.

$$\epsilon(\omega, q_x) = \epsilon_1(\omega, q_x) + \mathrm{i}\epsilon_2(\omega, q_x). \tag{12}$$

The optical properties in the present work are the refractive index, the absorption coefficient, and the extinction coefficient, given by [67-69]

$$n(\omega, q_x) = \sqrt{\frac{|\epsilon(\omega, q_x)| + \epsilon_1(\omega, q_x)}{2}}, \tag{13a}$$

$$\alpha(\omega, q_x) = \frac{\hbar\omega\epsilon_2(\omega, q_x)}{cn(\omega, q_x)}, \tag{13b}$$

$$\kappa(\omega, q_x) = \sqrt{\frac{|\epsilon(\omega, q_x)| - \epsilon_1(\omega, q_x)}{2}}. \tag{13c}$$

where c is the speed of the light (set to unity in our numerical calculations). In what follows we simplify the terms including the fermionic and bosonic Matsubara frequencies using the following approximations for $-3.5\,\mathrm{eV} \le \mathcal{E}/t_{p_z} \le +3.5\,\mathrm{eV}$ and $0\,\mathrm{eV} \le \hbar\omega/t_{p_z} \le 6\,\mathrm{eV}$,

$$\mathrm{i}\omega_{\mathcal{F}} \to \mathcal{E} + \mathrm{i}\eta, \tag{14a}$$

$$\mathrm{i}\omega_p \to \omega + \mathrm{i}\eta. \tag{14b}$$

4. Numerical results and discussions

We begin with some points about the optical quantities. The linear electron-light interactions are evaluated for the magnetic field perpendicular to aGNRs and aBNNRs. It is necessary to mention that the optical spectra are calculated for 1000×1000 unit cells with the broadening of about 30 meV. These abovementioned values are used either when the magnetic field is present. Furthermore, it has been assumed that the geometric structures of both lattices are optimized in the absence and presence of the magnetic field. Also, it should be noted that all optical quantities are calculated along the high-symmetry directions in the FBZ, originating from the p_z orbitals of carbon, boron, and nitrogen atoms. Now, we intend to describe the general treatments of $n(\omega,q_x)$, $\alpha(\omega,q_x)$, and $\kappa(\omega,q_x)$ briefly in order to handle the analyse of results easily.

In optics, the dimensionless number $n(\omega,q_x)$ stands for the index of refraction of a material describing how the path of incident light is refracted when entering the material. From this point, many features about the optical properties of the material can be obtained. For instance, $n(\omega,q_x)$ determines the amount of reflected light, the critical angle for total reflection, the phase velocity of light with respect to its vacuum value, the wavelength of propagating light in the material, the dispersion of light, and etc. It should be noted that the values of $n(\omega,q_x)$ must be below unity because of the theory of relativity. The light wave moving in the material (after crossing the interface) is typically a wave with the same frequency but shorter wavelength. This is a general explanation for $n(\omega,q_x)$. As for the ω-dependent $n(\omega,q_x)$, changes in the frequency of the incident light creates a disturbance in the electronic wave of each atom, leading to different responses from $n(\omega,q_x)$ at a fixed q_x transfer. Fig. 3 (a) shows the refractive index of different ultranarrow aGNRs and aBNNRs in the *absence* of magnetic field as a function of light frequency. The thermal energy and momentum transfer are fixed at $k_BT/t_{p_z} \simeq 0.25$ and $|q_xa_0| = \pi/6$ for all curves in Fig. 3. The static refractive index, i.e. $n(\omega,q_x)$ at $\omega = 0$ increases with the ribbon width for both lattices and in average one can see that the dynamical ones also increase with ribbon width in the whole energy range of $\hbar\omega/t_{p_z} \in [0-6]$. According to Fig. 3 (a), the main oscillations of the refractive index with the light start after the band gap energy of lattices, which is reasonable due to the interband transitions for $\hbar\omega/t_{p_z} > \mathcal{E}_{\mathrm{gap}}$. Generically, it can be seen that the maximum value for $n(\omega,q_x)$ occurs for 16-aBNNR at $\hbar\omega/t_{p_z} \simeq 2.5$, while this happens at $\hbar\omega/t_{p_z} \simeq 2$ for 7-aGNR. In short, all ribbon widths of aGNR and aBNNR do not show any refraction at high energies $\hbar\omega/t_{p_z} > 4.5$ because all curves approach zero independent of the ribbon width value.

Let us now turn to the absorption coefficient $\alpha(\omega,q_x)$. As known, for $\hbar\omega/t_{p_z} \ge \mathcal{E}_{\mathrm{gap}}$ the photon is absorbed, leading to the excitation of electrons from the valence bands to conduction bands. This absorption is shown by a probability of exciting, which manifests itself as a peak in adsorption coefficient quantity. The curve of $\alpha(\omega,q_x)$ tells us how far into a material, light can penetrate before absorption. Since the energy of light is important for exciting an electron, $\alpha(\omega,q_x)$ shows different behaviors at different $\hbar\omega/t_{p_z}$ strengths when the magnetic field is absent, as presented in Fig. 3 (b). As can be seen from this panel, for $\hbar\omega/t_{p_z} \ge 0.5$ and $\hbar\omega/t_{p_z} \ge 2.25$ corresponding to aGNRs and aBNNRs, respectively, the absorption peaks appear and the number of these

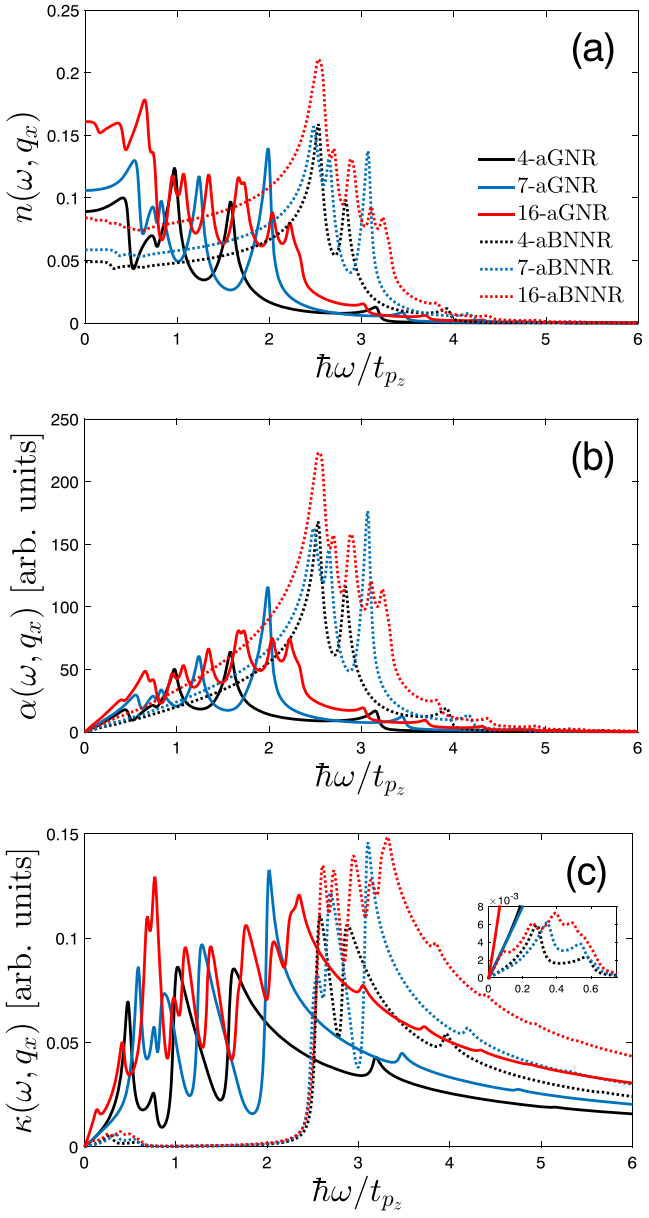

Fig. 3. (a) The refractive index, (b) the absorption coefficient, and (c) the extinction coefficient of aGNRs and aBNNRs in the *absence* of the magnetic filed for different ribbon widths. In all curves, the thermal energy and momentum transfer are fixed at $k_B T/t_{p_z} \simeq 0.25$ and $|q_x a_0| = \pi/6$, respectively.

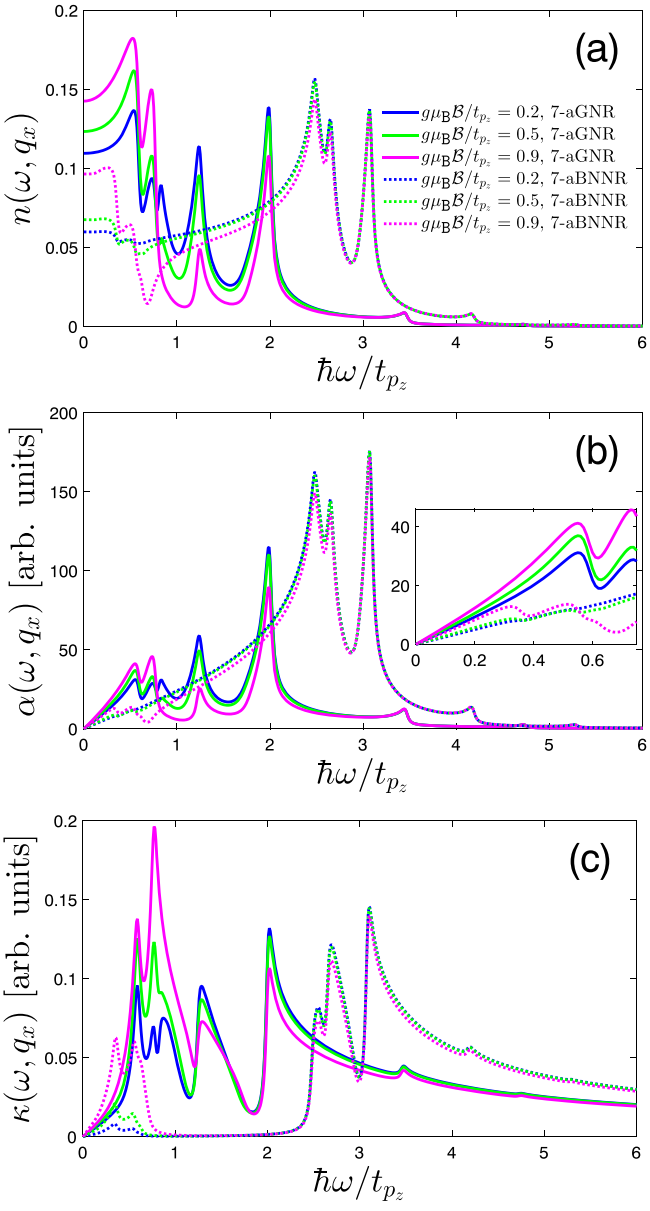

Fig. 4. The effect of magnetic field on the (a) refractive index, (b) absorption coefficient, and (c) extinction coefficient of 7-aGNRs and 7-aBNNRs at $k_B T/t_{p_z} \simeq 0.25$ and $|q_x a_0| = \pi/6$.

peaks increases with the ribbon width slightly for both lattices. Similarly, only interband transitions occur in $\alpha(\omega,q_x)$ spectra and there are no intraband transitions. Again, at $\hbar\omega/t_{p_z} \geq 4.5$ there are no peaks for both structures, which implies that the light cannot be absorbed for high enough energy of photons corresponding to shorter wavelengths. Among all six curves for different ribbon widths of aGNRs and aBNNRs, 16-aBNNR and 7-aGNR show the most absorptions at $\hbar\omega/t_{p_z} \simeq 2.5$ and $\hbar\omega/t_{p_z} \simeq 2$, respectively.

The extinction coefficient $\kappa(\omega,q_x)$ describes the decay or damping of the oscillation amplitude of the incident light wave. In fact, the measured transmittance of the light is controlled by the extinction coefficient, including both absorption and *scattering* coefficient, i.e. one can rewrite $\kappa(\omega,q_x) = \alpha(\omega,q_x) + \sigma(\omega,q_x)$ ($\sigma(\omega,q_x)$ being the scattering coefficient) [70]. That's why the curves of $\kappa(\omega,q_x)$ and $\alpha(\omega,q_x)$ are almost the same. However, the difference between them refers to the scattering process. According to Fig. 3 (c), the extinction coefficient for $g\mu_B\mathcal{B}/t_{p_z} = 0$ shows that the scattering of the host electrons from the light leads to the exotic features at low lying energy region. In other words, the intraband transitions come up at $\hbar\omega/t_{p_z} < 0.5$ and $\hbar\omega/t_{p_z} < 2.25$ corresponding to aGNRs and aBNNRs, respectively, which increase with the ribbon width when the magnetic field is not applied yet. For the curves above these frequencies, peaks at the same energies as the absorption coefficient appear but with different intensities and shapes originating from the scattering process. In general, the extinction coefficient scattering process in aGNRs and aBNNRs increases with the ribbon width.

Now, we proceed the investigation of the magneto-electron-light interaction in both lattices at a fixed ribbon width 7. There is no physical reason for this choice of ribbon width. The temperature and the incident wave vector are considered as before and the normalized magnetic field for both 7-aGNR and 7-aBNNR is changed from 0.2 to 0.9. Since we have detailed the physical meanings for quantities in the previous figure, we concisely will focus only on the analysis of results in the following.

In Fig. 4, the refractive index, absorption coefficient, and extinction coefficient of 7-aGNR and 7-aBNNR as a function of frequency at different Zeeman magnetic fields are displayed. Fig. 4 (a) presents the effect of magnetic field on $n(\omega,q_x)$ of 7-aGNR and 7-aBNNR. Surprisingly, the static refractive index increases with increasing the magnetic field in both lattices. On the other hand, the dynamical one increases with $g\mu_B\mathcal{B}/t_{p_z}$ up to $\hbar\omega/t_{p_z} \simeq 0.75$ and $\hbar\omega/t_{p_z} \simeq 0.5$, while it decreases within the frequency range $0.75 < \hbar\omega/t_{p_z} < 2$ and $0.5 < \hbar\omega/t_{p_z} < 2.5$ for 7-aGNR and 7-aBNNR, respectively. In other words, the refractive index changes with the magnetic field at low and intermediate frequencies. However, it is obvious that at high enough frequencies, i.e. $\hbar\omega/t_{p_z} > 2$ and $\hbar\omega/t_{p_z} > 2.5$ for 7-aGNR and 7-aBNNR, respectively, $n(\omega,q_x)$ does not change when the magnetic field becomes stronger. This can be understood from this fact that at high photon energies, the scattering rate of carriers is high and the magnetic field cannot change effectively the spatial distribution of electronic waves of carriers. Physically point of view, high photon energies correspond to higher and lower bands of electronic band structure (see Fig. 2) and since by increasing the magnetic field, the valence and conduction bands overlap, the impact of the magnetic field can be seen in intraband transitions much more than interband ones. We expect the same behaviors for other quantities after abovementioned threshold frequencies, as shown in panels (b) and (c).

As for the absorption coefficient of 7-aGNR and 7-aBNNR under the same condition as before, Fig. 4 (b) exhibits the frequency-dependent $\alpha(\omega,q_x)$ at $g\mu_B\mathcal{B}/t_{p_z} = 0.2$, 0.5, and 0.9. One can see that this coefficient increases with $g\mu_B\mathcal{B}/t_{p_z}$ up to $\hbar\omega/t_{p_z} \simeq 0.75$ and $\hbar\omega/t_{p_z} \simeq 0.5$, whereas it decreases at $0.75 < \hbar\omega/t_{p_z} < 2$ and $0.5 < \hbar\omega/t_{p_z} < 2.5$ corresponding to 7-aGNR and 7-aBNNR, respectively. Similar to the previous quantity $n(\omega,q_x)$, the magnetic field does not also affect the absorption coefficient of the systems. This implies that in addition to the frequency of the light, the probability of exciting depends strongly on the magnetic field strength. Indeed, the competition between the magnetic field potential and the photon energy determines the absorption process. This competition leads to the alterations only at low and intermediate ranges, not at high photon energies, i.e. $\hbar\omega/t_{p_z} > 2$ and $\hbar\omega/t_{p_z} > 2.5$ for 7-aGNR and 7-aBNNR, respectively. These results are in good agreement with Refs. [71,72] at low-energy regimes.

Finally, we finish the paper with studying the magneto-electron-light interaction in 7-aGNR and 7-aBNNR in Fig. 4 (c). As explained, we are interested in drawing the information about the scattering mechanism only in $\kappa(\omega,q_x)$ curves because of the similarity between the absorption and extinction coefficients. $\kappa(\omega,q_x)$ increases (decreases) with the magnetic field for $0 < \hbar\omega/t_{p_z} < 1.25$ ($1.25 < \hbar\omega/t_{p_z} < 3.5$) for 7-aGNR, while it increases slightly with $g\mu_B\mathcal{B}/t_{p_z}$ up to $\hbar\omega/t_{p_z} \simeq 1$ and does not alter for $\hbar\omega/t_{p_z} > 1$ for 7-aBNNR. These discrepancies stem from the scattering term $\sigma(\omega,q_x)$ in the extinction relation.

5. Conclusions

In this work, the linear optical responses in ultranarrow aGNRs and aBNNRs are investigated taking into account the effect of ribbon width and the Zeeman magnetic field using the linear response theory, tight-binding Hamiltonian model, and the Green's function technique. We observed different behaviors for refractive index, the absorption coefficient, and the extinction coefficient: (i) the static refractive index increases with both ribbon width and the magnetic field, while the dynamical refractive index increases (oscillates) in average, (ii) the absorption coefficient increases (oscillates), and (iii) the extinction coefficient introduces the scattering process of carriers when the ribbon width (magnetic field) is increased (applied). Generically, we found that high enough photon frequencies do not have effects on the optical responses significantly. These findings provide useful information to the experimentalists and engineers for future real applications of nanoribbons in order to select the best width and magnetic field strength for their main aims.

Acknowledgments

This research is funded by Vietnam's National Foundation for Science and Technology Development (NAFOSTED) under grant number 103.01-2017.361.

References

[1] A.K. Geim, K.S. Novoselov, The rise of graphene, Nat. Mater. 6 (2007) 183.
[2] F. Koppens, T. Mueller, P. Avouris, A. Ferrari, M. Vitiello, M. Polini, Photodetectors based on graphene, other two-dimensional materials and hybrid systems, Nat. Nanotechnol. 9 (2014) 780.
[3] Q. Bao, K.P. Loh, Graphene photonics, plasmonics, and broadband optoelectronic devices, ACS Nano 6 (2012) 3677.
[4] Y. Zhang, T. Liu, B. Meng, X. Li, G. Liang, X. Hu, Q.J. Wang, Broadband high photoresponse from pure monolayer graphene photodetector, Nat. Commun. 4 (2013) 1811.
[5] R. Saito, G. Dresselhaus, M.S. Dresselhaus, Physical Properties of Carbon Nanotubes, and references therein Imperial College Press, London, 1998.
[6] K. Wakabayashi, M. Fujita, H. Ajiki, M. Sigrist, Electronic and magnetic properties of nanographite ribbons, Phys. Rev. B 59 (1999) 8271.
[7] K. Nakada, M. Fujita, G. Dresselhaus, M.S. Dresselhaus, Edge state in graphene ribbons: nanometer size effect and edge shape dependence, Phys. Rev. B 54 (1996) 17954.
[8] M. Ezawa, Peculiar width dependence of the electronic properties of carbon nanoribbons, Phys. Rev. B 045432 (2006) 73.
[9] Y.W. Son, M.L. Cohen, S.G. Louie, Energy gaps in graphene nanoribbons, Phys. Rev. Lett. 216803 (2006) 97.
[10] N.M.R. Peres, A.H. Castro Neto, F. Guinea, Conductance quantization in mesoscopic graphene, Phys. Rev. B 195411 (2006) 73.
[11] D. Gunlycke, H.M. Lawler, C.T. White, Room-temperature ballistic transport in narrow graphene strips, Phys. Rev. B 75 (2007) 085418.
[12] H. Hsu, L.E. Reichl, Floquet-bloch states, quasienergy bands, and high-order harmonic generation for single-walled carbon nanotubes under intense laser fields, Phys. Rev. B 74 (2006) 115406.
[13] A.H. Castro Neto, N.M.R. Peres, K.S. Novoselov, A.K. Geim, The electronic properties of graphene, Rev. Mod. Phys. 81 (2009) 109.
[14] K. Wakabayashi, K. i. Sasaki, T. Nakanishi, T. Enoki, Electronic states of graphene nanoribbons and analytical solutions, Sci. Technol. Adv. Mater. 11 (2010) 054504.
[15] X. Li, X. Wang, L. Zhang, S. Lee, H. Dai, Chemically derived, ultrasmooth graphene nanoribbon semiconductors, Science 319 (2008) 1229.
[16] X. Jia, M. Hofmann, V. Meunier, B.G. Sumpter, J. Campos-Delgado, J.M. Romo-Herrera, H. Son, Y.P. Hsieh, A. Reina, J. Kong, M. Terrones, M.S. Dresselhaus, Controlled formation of sharp zigzag and armchair edges in graphitic nanoribbons, Science 323 (2009) 1701.
[17] X. Wang, H. Dai, Etching and narrowing of graphene from the edges, Nature Chem. 2 (2010) 661.
[18] S. Wang, L. Talirz, C.A. Pignedoli, X. Feng, K. Müllen, R. Fasel, P. Ruffieux, Giant edge state splitting at atomically precise graphene zigzag edges, Nat. Commun. 7 (2016) 11507.
[19] L. Talirz, P. Ruffieux, R. Fasel, On-surface synthesis of atomically precise graphene nanoribbons, Adv. Mater. 28 (2016) 6222.
[20] W.X. Wang, M. Zhou, X. Li, S.Y. Li, X. Wu, W. Duan, L. He, Energy gaps of atomically precise armchair graphene sidewall nanoribbons, Phys. Rev. B 93 (R) (2016) 241403.
[21] W. Xu, T.W. Lee, Recent progress in fabrication techniques of graphene nanoribbons, Mater. Horiz. 3 (2016) 186.
[22] C.S. Wu, J.D. Chai, Electronic properties of zigzag graphene nanoribbons studied by TAO-DFT, J. Chem. Theory Comput. 11 (2015) 2003.
[23] L. Talirz, H. Söde, T. Dumslaff, S. Wang, J.R. SánchezValencia, J. Liu, P. Shinde, C.A. Pignedoli, L. Liang, V. Meunier, N.C. Plumb, M. Shi, X. Feng, A. Narita, K. Müllen, R. Fasel, P. Ruffieux, On-surface synthesis and characterization of 9-atom wide armchair graphene nanoribbons, ACS Nano 11 (2017) 1380.
[24] Y.C. Chen, D.G. de Oteyza, Z. Pedramrazi, C. Chen, F.R. Fischer, M.F. Crommie, Tuning the band gap of graphene nanoribbons synthesized from molecular precursors, ACS Nano 7 (2013) 6123.
[25] M. Koch, F. Ample, C. Joachim, L. Grill, Voltage-dependent conductance of a single graphene nanoribbon, Nat. Nanotech. 7 (2012) 713.
[26] P.B. Bennett, Z. Pedramrazi, A. Madani, Y.C. Chen, D.G. de Oteyza, C. Chen, F.R. Fischer, M.F. Crommie, J. Bokor, Bottom-up graphene nanoribbon field-effect transistors, Appl. Phys. Lett. 253114 (2013) 103.
[27] M. Yarmohammadi, Perturbation tuning of plasmon modes in semiconductor armchair nanoribbons, Phys. Rev. B 98 (2018) 155424.
[28] B.D. Hoi, M. Yarmohammadi, Zeeman-magnetic-field-induced magnetic phase transition in doped armchair boron-nitride nanoribbons, EPL 122 (2018) 17005.
[29] B.D. Hoi, M. Davoudiniya, M. Yarmohammadi, On the intra-and interband plasmon modes in doped armchair graphene nanoribbons, Superlattice. Microst. 113 (2018) 576.
[30] W. Han, R.K. Kawakami, M. Gmitra, J. Fabian, Graphene spintronics, Nat. Nanotechnol. 9 (2014) 794.
[31] Y. Cai, G. Zhang, Y.W. Zhang, Polarity-reversed robust carrier mobility in monolayer MoS2 nanoribbons, J. Am. Chem. Soc. 136 (2014) 6269.
[32] C. Ataca, H. Şahin, E. Aktürk, S. Ciraci, Mechanical and electronic properties of

MoS2 nanoribbons and their defects, J. Phys. Chem. C 115 (2011) 3934.
[33] L. Sun, Y. Li, Z. Li, Q. Li, Z. Zhou, Z. Chen, J. Yang, J.G. Hou, Electronic structures of SiC nanoribbons, J. Chem. Phys. 129 (2008) 174114.
[34] D. Pacile, J.C. Meyer, C.O. Girit, A. Zettl, The two-dimensional phase of boron nitride: few-atomic-layer sheets and suspended membranes, Appl. Phys. Lett. 133107 (2008) 92.
[35] M. Corso, W. Auwarter, M. Muntwiler, A. Tamai, T. Greber, J. Osterwalder, Boron nitride nanomesh, Science 303 (5655) (2004) 217.
[36] K.S. Novoselov, D. Jiang, F. Schedin, T.J. Booth, V.V. Khotkevich, S.V. Morozov, A.K. Geim, Two-dimensional atomic crystals, Proc. Natl. Acad. Sci. (USA) 102 (2005) 10451.
[37] J.C. Meyer, A. Chuvilin, G. Algara-Siller, J. Biskupek, U. Kaiser, Selective sputtering and atomic resolution imaging of atomically thin boron nitride membranes, Nano Lett. 9 (2009) 2683.
[38] L. Brey, H.A. Fertig, Elementary electronic excitations in graphene nanoribbons, Phys. Rev. B 75 (2007) 125434.
[39] Z. Zhang, W. Guo, Energy-gap modulation of BN ribbons by transverse electric fields: first-principles calculations, Phys. Rev. B 77 (2008) 075403.
[40] C.H. Park, S.G. Louie, Energy gaps and stark effect in boron nitride nanoribbons, Nano Lett. 8 (2008) 2200.
[41] J. O'Keeffe, C.J. Wei, K.J. Cho, Bandstructure modulation for carbon nanotubes in a uniform electric field, Appl. Phys. Lett. 80 (2002) 676.
[42] Y.W. Son, J. Ihm, M.L. Cohen, S.G. Louie, H.J. Choi, Electrical switching in metallic carbon nanotubes, Phys. Rev. Lett. 95 (2005) 216602.
[43] C.W. Chen, M.H. Lee, S.J. Clark, Band gap modification of single-walled carbon nanotube and boron nitride nanotube under a transverse electric field, Nanotechnology 15 (2004) 1837.
[44] Y.H. Kim, K.J. Chang, Electronic structure of radially deformed BN and BC 3 nanotubes, Phys. Rev. B 64 (2001) 153404.
[45] Y. Li, S.V. Rotkin, U. Ravaioli, Electronic response and bandstructure modulation of carbon nanotubes in a transverse electrical field, Nano Lett. 3 (2003) 183.
[46] T.S. Li, M.F. Lin, Electronic properties of carbon nanotubes under external fields, Phys. Rev. B 73 (2006) 075432.
[47] K.H. Khoo, M.S.C. Mazzoni, S.G. Louie, Tuning the electronic properties of boron nitride nanotubes with transverse electric fields: a giant dc Stark effect, Phys. Rev. B 69 (R) (2004) 201401.
[48] V. Barone, J.E. Peralta, Magnetic boron nitride nanoribbons with tunable electronic properties, Nano Lett. 8 (2008) 2210.
[49] C.H. Park, S.G. Louie, Energy gaps and stark effect in boron nitride nanoribbons, Nano Lett. 8 (2008) 2200.
[50] T. Takenobu, Y. Murayama, Y. Iwasa, Optical evidence of Stark effect in single-walled carbon nanotube transistors, Appl. Phys. Lett. 89 (2006) 263510.
[51] M. Ishigami, J.D. Sau, S. Aloni, M.L. Cohen, A. Zettl, Observation of the giant stark effect in boron-nitride nanotubes, Phys. Rev. Lett. 94 (2005) 056804.
[52] Y.W. Son, M.L. Cohen, S.G. Louie, Half-metallic graphene nanoribbons, Nature (London) 444 (2006) 347.
[53] Y. Cai, L. Zhang, Q. Zeng, L. Cheng, Y. Xu, Infrared reflectance spectrum of BN calculated from first principles, Solid State Commun. 141 (2007) 262.
[54] V. Gusynin, V. Miransky, S. Sharapov, I. Shovkovy, Edge states in quantum Hall effect in graphene (Review Article), Low, Temp. Phys. 34 (2008) 778.
[55] V.P. Gusynin, V.A. Miransky, S.G. Sharapov, I.A. Shovkovy, C.M. Wyenberg, Edge states on graphene ribbons in magnetic field: interplay between Dirac and ferromagnetic-like gaps, Phys. Rev. B 79 (2009) 115431.
[56] I.V. Zagorodnev, Z.A. Devizorova, V.V. Enaldiev, Resonant electron scattering by a graphene antidot, Phys. Rev. B 92 (2015) 195413.
[57] C.Y. Lin, J.Y. Wu, C.P. Chang, M.F. Lin, Electronic and optical properties of graphite-related systems, Carbon 69 (2014) 151.
[58] X. Chen, K. Song, B. Zhou, H. Wang, G. Zhou, Scanning tunneling microscopy image modeling for zigzag-edge graphene nanoribbons, Appl. Phys. Lett. 98 (2011) 093111.
[59] S. Wu, B. Liu, C. Shen, S. Li, X. Huang, X. Lu, P. Chen, G. Wang, D. Wang, M. Liao, J. Zhang, T. Zhang, S. Wang, W. Yang, R. Yang, D. Shi, K. Watanabe, T. Taniguchi, Y. Yao, W. Wang, G. Zhang, Magnetotransport properties of graphene nanoribbons with zigzag edges, Phys. Rev. Lett. 120 (2018) 216601.
[60] X. Chen, K. Song, B. Zhou, H. Wang, G. Zhou, Semiconducting states and transport in metallic armchair-edged graphene nanoribbons, J. Phys.: Conden. Matter 23 (2011) 315304.
[61] K. Zhao, M. Zhao, Z. Wang, Y. Fan, Tight-binding model for the electronic structures of SiC and BN nanoribbons, Physica E 43 (2010) 440.
[62] K. Wakabayashi, Y. Takane, M. Yamamoto, M. Sigrist, Electronic transport properties of graphene nanoribbons, New J. Phys. 11 (2009) 095016.
[63] C.Y. Lin, J.-Y. Wu, C.P. Chang, M.F. Lin, Optical properties of graphene in magnetic and electric fields, arXiv:1603.02797 [physics. comp-ph].
[64] H. Zheng, Z.F. Wang, T. Luo, Q.W. Shi, J. Chen, Analytical study of electronic structure in armchair graphene nanoribbons, Phys. Rev. B 75 (2007) 165414.
[65] D. Prezzi, D. Varsano, A. Ruini, E. Molinari, Quantum dot states and optical excitations of edge-modulated graphene nanoribbons, Phys. Rev. B 84 (R) (2011) 041401.
[66] G.D. Mahan, Many Particle Physics, Plenum Press, New York, 1993.
[67] T. Ando, Y. Zheng, H. Suzuura, Dynamical conductivity and Zero-Mode anomaly in honeycomb lattices, J. Phys. Soc. Jpn. 71 (2002) 1318.
[68] R. Beiranvand, S. Valedbagi, Electronic and optical properties of h-BN nanosheet: a first principles calculation, Diamond Relat. Mater. 58 (2015) 190.
[69] S. Behzad, Ab-initio calculation of electronic structure and optical properties of AB-stacked bilayer -graphyne, Phys. E 83 (2016) 211.
[70] C. Backes, R.J. Smith, N. McEvoy, N.C. Berner, D. McCloskey, H.C. Nerl, A. O'Neill, P.J. King, T. Higgins, D. Hanlon, N. Scheuschner, J. Maultzsch, L. Houben, G.S. Duesberg, J.F. Donegan, V. Nicolosi, J.N. Coleman, Edge and confinement effects allow in situ measurement of size and thickness of liquid-exfoliated nanosheets, Nat. Commun. 5 (2014) 4576.
[71] H. Chung, C. Chang, C.Y. LIN, M. Lin, Electronic and optical properties of graphene nanoribbons in external fields, Phys. Chem. Chem. Phys. 18 (2015) 7573.
[72] J. Have, T.G. Pedersen, Magnetoexcitons and Faraday rotation in single-walled carbon nanotubes and graphene nanoribbons, Phys. Rev. B 97 (2018) 115405.